Single-Particle Momentum Distributions from Deep Inelastic Neutron Scattering (DINS) *

Ralph O. Simmons

Physics Department and Materials Research Laboratory, University of Illinois at Urbana-Champaign, USA

Z. Naturforsch. **48a**, 415–424 (1993); received December 27, 1991

Single-particle longitudinal momentum distributions in condensed matter are now accessible to direct measurement using eV neutrons. Some systems of particular interest include a) quantum solids and fluids, formed from ^{3}He, ^{4}He, and H_2, b) prototype molecular crystals, formed from noble gases, c) fluids such as H_2 and Ne, which show deviations from classical behavior and d) mixed systems, in which guest-host interactions may be important. Quantum solids can be investigated at substantially different densities, for different structures, and further, can be compared to the corresponding fluids, with which they have significant similarities in their single-particle properties such as their momentum distributions. Noble gas solids comprise a graduated family with progressively varying importance of zero-point energy, of phonon anharmonicity, and of multi-body forces. They have also been very useful for matrix isolation studies, and eV neutron scattering can yield their center-of-mass motions, not previously seen directly. Finally, noble gas fluids can be used to investigate the nature and extent of final-state effects in the neutron scatttering. Such effects are defined to be the difference between the longitudinal "neutron Compton profile" and the longitudinal momentum distribution.

Key words: Momentum distribution; Dynamics; Neutron scattering.

PACS Nos. 61.12.Gz, 63.20.-e, 61.25.Bi.

I. Principles of the Method

Advances in understanding physical systems have often been made through the use of scattering techniques. To study atomic structure, the Geiger-Marsden alpha-particle experiments [1] relied upon elastic scattering, and Rutherford analyzed the distribution of momentum transfers [2]. Much subsequent work in various branches of physics and chemistry has concentrated upon inelastic scattering at a given momentum transfer, with analysis of the distribution of energy transfers.

The discovery of the (inelastic) Compton effect [3] provided a direct tool for the study of electronic structure, which was exploited brilliantly by DuMond and Kirkpatrick [4]. Figure 1 a shows the principle schematically. The Compton relation giving a photon frequency shift (energy transfer) at a given scattering angle (momentum transfer) gives the location of the Compton peak, ω_c (for a target electron initially at rest). For a collection of target electrons in a given atomic state, that is, with an initial momentum distribution $n(\boldsymbol{p})$, the observed Compton peak is broadened into a Compton profile, which can be related to $n(\boldsymbol{p})$.

In principle, neutrons can be used to carry out analogous direct studies of atomic momentum distributions. Figure 1 b shows the analogy; $\boldsymbol{Q}$ is the wave-vector transfer and $E = \hbar\omega$ is the energy transfer. Use of this method was impractical, however, until the advent of pulsed neutron sources provided a sufficient flux of the epithermal neutrons necessary to impart the large energy transfers required.

The neutron inelastic scattering cross-section is related to the dynamic structure factor $S(\boldsymbol{Q}, \omega)$ by [5]

$$\frac{\mathrm{d}^2\sigma}{\mathrm{d}\Omega\,\mathrm{d}\omega} = (k_\mathrm{f}/k_\mathrm{i})\, b^2\, S(\boldsymbol{Q}, \omega)\,, \tag{1}$$

where b is a scattering length, k_f and k_i are final and initial neutron wave vectors, respectively, and Ω is the solid angle. $S(\boldsymbol{Q}, \omega)$ contains the information of interest about the system. Figure 2 shows this schematically for scattering by two different atoms. For a liquid or solid, at small energy and momentum transfers the

* Supported by the U.S. Department of Energy, BES-Materials Sciences under Grant DEFG02-91ER45439.

Presented at the Sagamore X Conference on Charge, Spin and Momentum Densities, Konstanz, Fed. Rep. of Germany, September 1–7, 1991.

Reprint requests to Prof. R. O. Simmons, University of Illinois, Physics Department, 1110 West Green Street, Urbana, IL 61801, USA.

0932-0784 / 93 / 0100-0415 $ 01.30/0. – Please order a reprint rather than making your own copy.

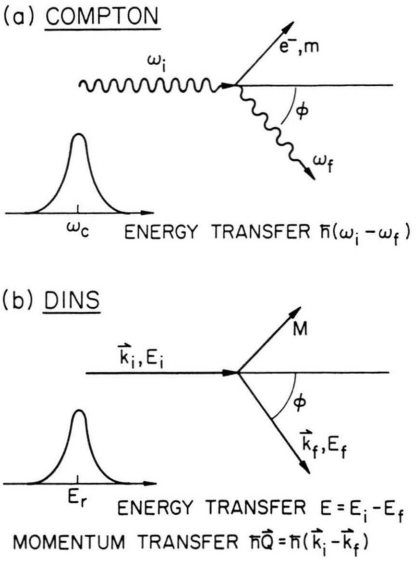

Fig. 1. Schematic comparison of photon Compton scattering and of deep inelastic neutron scattering (DINS). See text Section I.

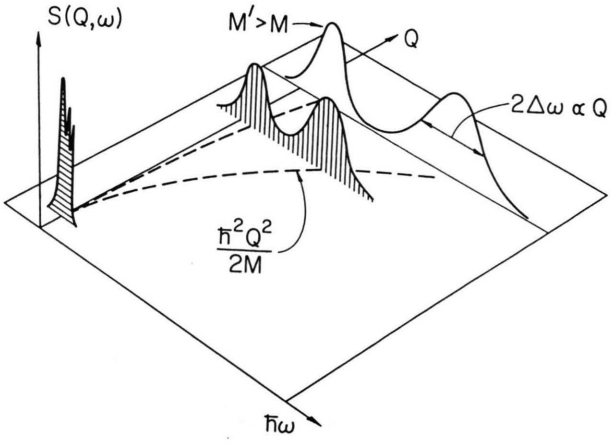

Fig. 2. The neutron response $S(Q, \omega)$ at large wave-vector transfer Q becomes single peaks, each centered around a recoil energy corresponding to the nucleus involved. See text Sect. I and Figure 9.

structure of $S(\boldsymbol{Q}, \omega)$ is rich in information, about collective excitations, about particle diffusion, and so on. Thermal neutrons from reactors have energies and associated wavelengths well-matched to such phenomena and have been much used; Figure 2 does not illustrate this complexity in detail. Rather, the figure emphasizes the region of present interest, at large Q and large ω. In this region of deep inelastic scattering, $S(\boldsymbol{Q}, \omega)$ takes a simple form. For each nuclear mass there is a peak, broadened and shaped by dynamical effects. At a given (large) Q, a peak is centered about an energy transfer $E_r = \hbar\omega_r = \hbar^2 Q^2/2M$, the recoil energy of an initially stationary atom of mass M. For each collection of masses M in the target, in motion with a momentum distribution $n(\boldsymbol{p})$, the corresponding peak is broadened by an amount approximately proportional to Q.

These general features of the method are well known, but it is taking some time for practical understanding of the conditions, required for precise interpretation of experimental data. The regime of deep inelastic scattering is defined to be that for which $Q \gg 2/R$, where R is the distance to nearest-neighbors of the target atom in the condensed matter system. In this regime, it is appropriate to calculate $S(\boldsymbol{Q}, \omega)$ in an incoherent approximation, which regards each atom as scattering independently of other atoms. In the limit of infinite Q, $S(\boldsymbol{Q}, \omega)$ becomes proportional to the thermodynamic average of a delta function that expresses conservation of energy and momentum in a single-particle collision,

$$S_\infty(\boldsymbol{Q}, \omega) = \int n(\boldsymbol{p})\, \delta(\omega - \omega_r - \boldsymbol{Q} \cdot \boldsymbol{p}/M)\, \mathrm{d}\boldsymbol{p}\,. \quad (2)$$

The momentum distribution in this expression is normalized, so that the fraction of atoms in the initial state with momenta $\boldsymbol{p}$ in $\mathrm{d}\boldsymbol{p}$ is $n(\boldsymbol{p})\, \mathrm{d}\boldsymbol{p}$. In this high-$Q$ limit, we invoke the impulse approximation [6], and the scattering atom recoils as if it were free, i.e., interatomic forces are neglected in the final state of the scattering process. Of course, the presence of such forces in the *initial* state is what produces a momentum distribution of interest.

The practical problem involves determining the degree to which the conditions of the impulse approximation apply to a given set of experimental data, and how to correct for final-state interactions, if any. Scaling methods are a powerful tool to apply [7]. A useful framework for analysis of data on neutron scattering by isotropic systems was presented by Sears [8]. One defines the scaling variable

$$y = (M/Q)\,(\omega - \omega_r)\,. \quad (3)$$

One then sees that

$$S(\boldsymbol{Q}, \omega) = (M/Q)\, J(y)\,, \quad (4)$$

where $J(y)$ is the longitudinal momentum distribution function,

$$J(p_z) = \int_{-\infty}^{\infty} \int_{-\infty}^{\infty} n(p_x, p_y, p_z)\, \mathrm{d}p_x\, \mathrm{d}p_y\,, \quad (5)$$

with $y \parallel Q$. In Compton scattering, $J(y)$ is the Compton profile referred to in Figure 1 a.

Sears writes an expression for an isotropic $S(Q, \omega)$ as a series expansion of the derivatives of J,

$$S(Q, \omega) = \left(\frac{M}{Q}\right) \sum_{n=0}^{\infty} (-1)^n A_n(Q) \frac{d^n J(y)}{dy^n}, \quad (6)$$

and calculates formal expressions for the coefficients $A_n(Q)$. For an isotropic scattering system, $A_0 = 1$ and A_1 and A_2 are both zero. Then (6) becomes

$$S(Q, \omega) = \left(\frac{M}{Q}\right)\left[1 + \sum_{n=3}^{\infty} (-1)^n A_n(Q) \frac{d^n}{dy^n}\right] J(y). \quad (7)$$

Sears gives explicit expressions for A_3 and A_4,

$$A_3(Q) = M \langle \Delta^{(2)} V \rangle / 36 \hbar^2 Q, \quad (8)$$

$$A_4(Q) = M^2 \langle \nabla V \cdot \nabla V \rangle / 72 \hbar^4 Q^2, \quad (9)$$

and Belić and Pandharipande [9], discussing the antisymmetric part of $S(Q, \omega)$ and using sum rules, for A_5. If the interatomic potential, V, is known (such as is the case for helium at not too high density, where the interactions are pairwise), and the structure is known, then these coefficients can be calculated. (See [9] for an application to liquid ^{4}He.)

For an isotropic Gaussian $S_\infty(Q, \omega)$ both $n(p)$ and $J(y)$ are also of Gaussian form. The characteristic Gaussian width of $S_\infty(Q, \omega)$ is

$$\Delta\omega = \left(\frac{8 \ln 2}{3}\right)^{1/2} \left(\frac{p_0}{M}\right) Q, \quad (10)$$

which is proportional to Q as noted in Fig. 1 b, and p_0 is the rms momentum.

On the other hand, if $S(Q, \omega)$ has sharp features, such as are expected in scattering by superfluid ^{4}He, then the formal expansion (7) is of limited usefulness. Here we consider physical systems for which no such sharp features are expected.

In Fig. 3, these effects are illustrated for a model of liquid Ne for $Q = 100\ \mathrm{nm}^{-1}$, near the practical limit for reactor neutron work (because of the dearth of high-energy neutrons). A Gaussian $J_\infty(y)$ is shown, having a width near that of actual measurements on Ne at 27 K. Also shown are curves representing the first asymmetric (8) and next symmetric (9) terms. From these curves, it can be seen that appreciable asymmetry, and possibly some narrowing, is to be expected in the measured response, compared to a strict Gaussian shape.

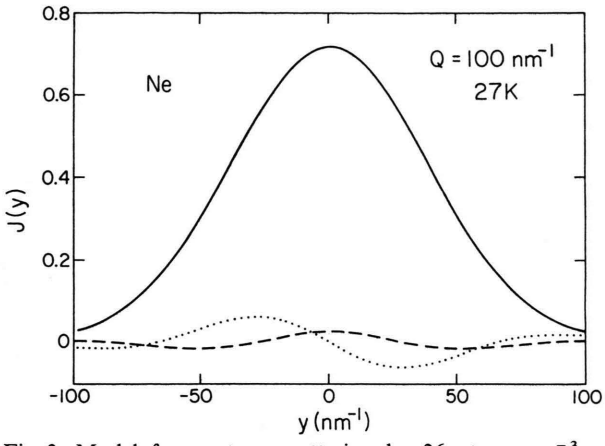

Fig. 3. Model for neutron scattering by 36 atoms nm^{-3} liquid Ne at 27 K, for the moderate wave-vector transfer $Q = 100\ \mathrm{nm}^{-1}$. A Gaussian response $J_\infty(y)$ is shown (full), corresponding to a Gaussian momentum distribution $n(p)$. But at this moderate Q, it is expected that other contributions to the response are appreciable. The largest are antisymmetric (dotted) and higher-order symmetric (dashed), calculated from (8) and (9), respectively. It is therefore desirable to take data at much larger Q.

Consideration of final-state effects in deep inelastic neutron scattering has continued to be an active theoretical field [10]. And on the experimental side it is fair to say, without space here to elaborate, that while suggestive results about possible final-state effects have been obtained, no absolutely conclusive publications have yet appeared in the area of experimental ^{4}He studies spanned by work from 1974 [11] to the present [12].

II. Chopper Spectrometers at a Pulsed Neutron Source

A chopper spectrometer is often the instrument of choice for measurements of $S(Q, \omega)$ at a pulsed neutron source, when relatively high resolution is required at large energy transfer $\hbar\omega$ [13]. The source produces neutrons by spallation from a suitable target (uranium, tungsten) struck by pulsed protons and surrounded by a moderator/reflector which shapes the neutron energy distribution. At the spectrometer, neutrons incident on the sample are selected by a Fermi chopper synchronized with the pulsed protons. Detectors placed at known scattering angles register the scattered neutrons, whose energies are determined through time of flight from the sample.

An example of first-generation raw time-of-flight data of Hilleke [14] is shown in Figure 4. The sample

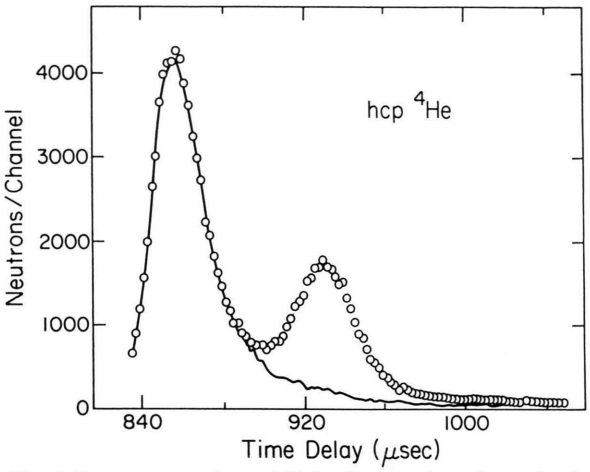

Fig. 4. Raw neutron time-of-flight data per 2 μs channel collected in a detector group centered at a scattering angle of 96.9° for incident neutrons having energy 505 meV [14]. The sample is hcp crystal ^{4}He at a density of 30.9 atoms nm^{-3}. The ^{4}He energy transfer peaks at a value corresponding to Q about 200 nm^{-1}. Compare the shaded region of Fig. 2 at high Q.

is solid hcp ^{4}He contained at a pressure of 5.41 MPa within a cylindrical aluminum shell. At a given scattering angle, two peaks are seen. The faster neutrons (at shorter time delay) lost less energy, having scattered from the aluminum. The solid line shows the scattered-neutron counts (normalized to the same incident flux) when the aluminum cell is empty. The difference then represents the sample scattering (1), as broadened and otherwise affected by finite resolution of the spectrometer and sample-dependent multiple scattering [15]. Note that the background Al peak is well separated kinematically from that of the ^{4}He sample; such helpful separation does not occur in traditional inelastic scattering measurements using thermal neutrons.

As theoretical simulations of condensed-matter systems have become more refined, and as neutron source intensities have increased, it has become worthwhile to treat data in more detail. The work of Blasdell [16], for example, shows the importance of careful instrument simulation in precise second-generation work with time-of-flight spectrometers, as one searches at high Q for indications of the higher-order effects represented in (7)–(9). Blasdell's simulation works with the actual neutron time-of-flight trajectories, but the results are presented for convenience as $J(y)$.

It would be desirable to report all measurements in the form of the intrinsic $S(Q, \omega)$ or $J(y)$. For high-Q work with a chopper spectrometer this is hardly possible, however, even with polycrystalline samples, because in precise data analysis the instrument simulation and the allowance for possible final-state effects enter in different fashions. Even in an ideal case of data without statistical noise and without sample-dependent background, a fully self-consistent procedure such as that described by Sears [8], which decomposes an observed $S(Q, \omega)$ into symmetric and antisymmetric parts, is impractical. In these circumstances, the best tactic for systems having a simple $S(Q, \omega)$ appears to be intervention of a model, such as that given by the Sears expansion (6).

III. Resonance Filter Neutron Spectrometers

Another method to measure DINS spectra is by use of a nuclear-resonance filter-difference spectrometer [17]. Compared to current chopper spectrometers, this method at a pulsed neutron source can employ larger values of Q and ω. On the other hand, the measured recoil spectrum is convoluted with a complicated instrument resolution function dependent upon both geometrical details of the spectrometer and several assumptions. Precise work demands great care in collecting data and subtracting to find the difference spectra. For example, anisotropy in the proton momentum distribution in $KHCO_3$ has been reported [18]. Interesting further applications of this method are described elsewhere in these Proceedings [19].

IV. Some Systems of Interest

A) Quantum Solids and Liquids

A major motivation for DINS studies has been the search for a Bose condensate in superfluid ^{4}He. Limited space precludes consideration of this rather controversial subject here [20]. Rather, this section primarily treats properties of "quantum" solids, for which the de Broglie wavelength associated with ground-state atomic momentum is comparable to the interatomic spacing R. For such solids, a) the amplitude of atomic vibrational motion, $\langle u^2 \rangle^{1/2}$, is a significant fraction of R, and b) the effects of vibrational anharmonicity are expected to be large. The first publication of DINS results on solid ^{4}He was in 1984 [21].

1. Vibrational Anharmonicity

Anharmonicity may be evident from *inequality* of the kinetic- and potential-energy parts of the ground-

state energy. Para-H_2 at saturated vapor pressure has the large ratio $\langle u^2\rangle^{1/2}/R = 0.18$, according to thermal neutron scattering measurements [22], and thus anharmonicity may be significant. Such inequality has been found for solid para-H_2 by Langel et al. [23], in which the directly measured $\langle E_k\rangle$ is about 60% of the total ground-state energy, not a harmonic 50%.

2. Density Variation of $\langle E_k\rangle$

Quantum solids are convenient for the study of effects over wide ranges of density, because they are highly compressible. Such large relative variations in atomic density are not accessible in usual solids (nor for valence electrons in photon Compton work). For the single-particle kinetic energy $\langle E_k\rangle$, the density dependence can be large. The strong dependence of $\langle E_k\rangle$ is illustrated by a rough estimate that uses a) a harmonic Debye model to represent the crystal vibrations, for which the ground-state kinetic energy is

$$\langle E_k\rangle = (9/16)\,\Theta\,. \tag{11}$$

and b) a lumped-lattice Grüneisen parameter, γ_L, to represent the dependence upon density, ϱ, of the characteristic Debye energy $\hbar\omega = k\Theta$,

$$\mathrm{d}\langle E_k\rangle/\langle E_k\rangle = \gamma_L\,\mathrm{d}\varrho/\varrho\,. \tag{12}$$

Para-hydrogen was studied by Herwig and coworkers [24] in a thick pressure cell, over a one-third variation in density. Shown in Fig. 5 are the results of the measurements, as well as the low-density $\langle E_k\rangle$ value of Langel et al. [23], collected in a thin-wall cell that permitted easier background subtraction. Comparison of these data to model expectations is also shown. The simple model (11) with Θ values from calorimetry on samples at different volumes [25] yields $\langle E_k\rangle$ values smaller than the measured ones, a result which is also found for hcp ^{4}He [26]. In better agreement with experiment are the early Monte Carlo (MC) calculations of Bruce [27], which follow the trend of the data both in magnitude and density dependence.

The very strong dependence of $\langle E_k\rangle$ upon particle density, characteristic of a quantum system, is also present in the fluid phase (see Table 1, showing that at constant density, fluid and solid $\langle E_k\rangle$ values for ^{4}He are closely similar). When this strong variation in the width of $S(Q, \omega)$ is not taken into account, erroneous deductions can follow. An example are measurements on saturated liquid ^{4}He at varying temperatures (and therefore also varying densities) [28].

Table 1. Comparison of experimental and theoretical values for $\langle E_k\rangle$ for condensed ^{4}He. Experimental values are from Blasdell and Simmons [30] and theoretical values are PIMC calculations of Ceperley [30, 31].

Phase	T (K)	$\langle E_k\rangle$ (K)	
		Experiment	Theory
bcc	1.725	23.65	–
	1.67	–	24.08
hcp	1.070	23.58	–
(fcc)	1.60	–	24.40
Liquid	2.35	–	24.75
	2.70	24.23	–
	4.00	–	25.66

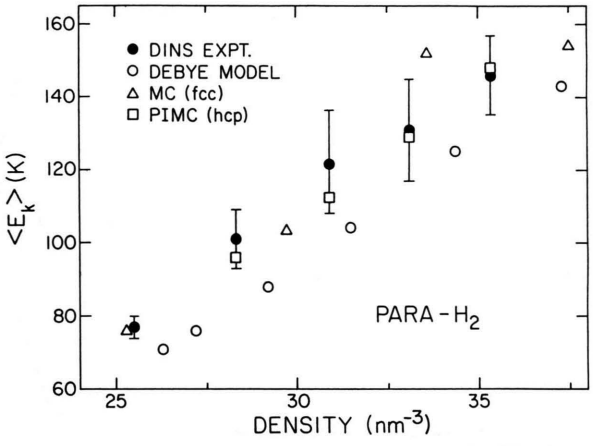

Fig. 5. Density dependence of $\langle E_k\rangle$ for para-H_2. The hcp phase experimental points are from [23] and [24]. The open circles represent the Debye model (11). The triangles are MC calculations [27], while the squares are results, extrapolated to high Trotter number, of PIMC simulations using the same Mie-Lennard-Jones pair potential [34].

3. $\langle E_k\rangle$ in Different Structures

An extraordinary possibility, with condensed helium, is the study of single-particle dynamics in a quantum system at constant particle density (to remove the density effects noted in Sect. IV.A.2) while the system is prepared in different structures. For ^{4}He at a density near 28.8 atoms nm^{-3}, such preparation is possible by adjustments of the temperature and applied pressure. Early data on ^{4}He samples of this kind suggested that $\langle E_k\rangle$ is largely independent of whether the sample is solid or liquid (at constant density) [29].

Precise measurements on ^{4}He hcp, bcc, and liquid samples at fixed density have now been made by Blasdell [30]. In this work, special care was given to char-

acterize the structure of the crystalline samples by diffraction. The results are shown in Table 1. They show that, indeed, particle density, not structure, dominates the value of $\langle E_k \rangle$.

Sophisticated path-integral MC (PIMC) simulations of different ^{4}He phases at finite temperature are now available. Ceperley's results [31] are also shown in Table 1. Generally, his calculations also show that at constant density the value of $\langle E_k \rangle$ is little affected by change of phase. Whether the measurements and the calculations disagree, outside the sum of their respective estimated uncertainties, is another question, still under investigation.

4. Crystalline Anisotropy in $n(\boldsymbol{p})$?

The relations (3)–(10) apply to isotropic systems like fluids. But one may ask to what extent crystalline systems may have anisotropy in $n(\boldsymbol{p})$ and hence in the observed $S(\boldsymbol{Q}, \omega)$. For example, current theory for crystallline He does not provide much guidance; the calculated distributions are spherical averages.

One has two experimental alternatives. The first is to search explicitly for DINS anisotropy from a single-crystal sample [32]. In He, only one such search has been reported [33]. In order to minimize uncertainties due to variation of spectrometer resolution and of multiple scattering with scattering angle, scattering from a liquid sample was compared to that from a single crystal of hcp ^{4}He, the c-axis of which lay in the scattering plane. The relative widths of the scattering functions were found to be independent of scattering angle (that is, of the direction of $\boldsymbol{Q}$ and hence, from the kinematics, of the direction of $\boldsymbol{p}$ in the crystal) over a full range including both c-axis and a-axis orientations, within experimental uncertainties of about 5%. The second alternative is deliberately to use a polycrystalline sample having a range of crystallite orientations. This strategy has been adopted for most work by the Illinois group. Its most complete verification, through detailed diffraction work on polycrystalline He samples, has been by Blasdell [30].

5. Other Comments

For hcp ^{4}He, final-state effects in the neutron scattering process are being investigated through experimental determination of the coefficients A_3 and A_4, (8) and (9), respectively [30]. At a given Q, these coefficients depend upon spatial averages of the Laplacian of the potential energy. Qualitatively, one expects that such averages will increase in value as the particle density of the system is increased. This kind of variation is found, at least for A_3.

The availability of direct measurements of single-particle kinetic energies is stimulating sophisticated calculations. Besides the ^{4}He example shown in Table 1, another example is a PIMC simulation of solid para-H_2 [34], shown in Fig. 5, where excellent agreement is demonstrated with experiment. More efficient techniques for MC simulation continue to be developed [35].

B) Noble-Gas Systems

1. The Heavier Systems Ar, Kr, Xe

Massive elements such as condensed Ar and beyond might seem unpromising for DINS study because of the limited recoil energies that can be imparted using eV neutrons. However, for these weakly-bound fcc solids, values of $\langle u^2 \rangle^{1/2}/R$ are thought to be appreciable, especially at high temperature. (There are no published values of $\langle u^2 \rangle$ from direct measurement, aside from some inferences about Kr from Mössbauer spectroscopy). Clean DINS data can be obtained on these elements, as shown in Fig. 6 for solid Ar [36].

At high temperatures, DINS data on solid and liquid Ar, Kr, and Xe give an explicit demonstration that "Boltzmann was right". That is, equipartition of energy predicts that for a classical system in thermal equilibrium, regardless of a) its density, b) its phase (solid or fluid), or c) the nature of the interactions between its particles, each degree of freedom contributes precisely $(1/2)k_bT$ to the kinetic energy. Of course, the total energy depends upon all these factors a)–c). The excellent agreement between direct measurements of $\langle E_k \rangle$ and the expected $(1/2)k_bT$ energy per degree of freedom is shown in Table 2, which contains data of Peek [36] and of Fradkin and Zeng [37]. Note that both solid and liquid phases are represented, and there is a wide range of particle densities.

The capacity of the DINS method is thereby proven to yield $\langle E_k \rangle$ values even for heavy nuclei. The way is therefore open in principle to use DINS as a test for particle thermal equilibrium and for other purposes.

A final pedagogic demonstration is available from DINS data on the family of condensed noble gases. These elements have often served as prototype systems for analysis of corresponding states, when phys-

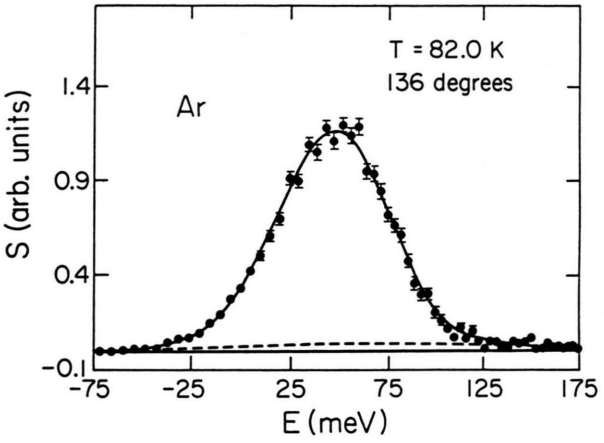

Fig. 6. DINS peak for solid Ar near melting, for an incident neutron energy of 500 meV [36]. The peak is broadened by the distribution of atomic momenta and by finite instrumental resolution. Sample-dependent background is represented by a small quadratic polynomial (dashed) employed in the fitting of a Gaussian peak to the scattering at the fixed angle of 136°. Unlike the situation for He shown in Fig. 4, the Al cell peak lies very near the Ar sample peak.

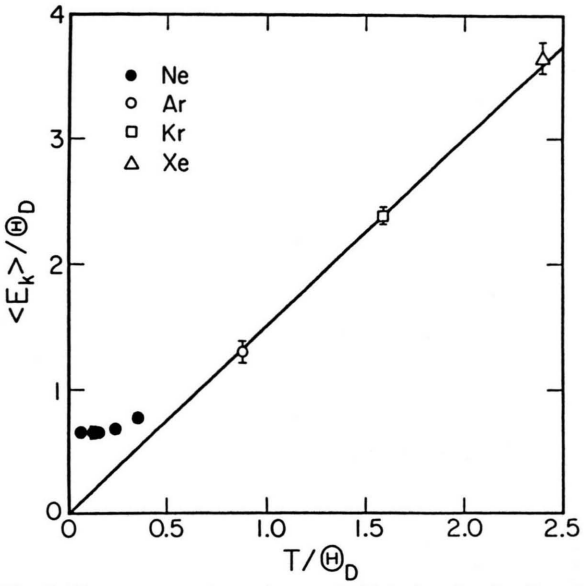

Fig. 7. Temperature dependence of $\langle E_k \rangle$ for the family of noble-gas solids [36]. To show corresponding behavior, the plot is reduced using characteristic temperatures of 74.6, 93.1, 72.1, and 64.0 K for the four elements Ne (●), Ar (○), Kr (□), and Xe (△), respectively.

Table 2. The single-particle kinetic energy, $\langle E_k \rangle$, follows the equipartition of energy, (3/2) $k_b T$ in the monatomic systems Ar, Kr, and Xe at high temperatures, T, where classical conditions are expected. This result is independent of phase and of density.

Element	Phase	Density (atoms nm^{-3})	T (K)	(3/2) T (K)	$\langle E_k \rangle$ (K)
Ar	solid [a]	24.5	82.0	123	121 ± 8
Ar	liquid [b]	21.2	84.9	127	129 ± 2 [c]
Kr	solid [a]	20.3	114.7	172	172 ± 5
Kr	liquid [a]	17.6	119.4	179	178 ± 6
Xe	solid [a]	15.8	153.4	230	234 ± 8
Xe	liquid [a]	11.6	221.3	332	348 ± 23

[a] Ref. [36]. – [b] Ref. [37].
[c] For liquid Ar at this temperature, one expects small positive quantum corrections to be present [F. Barocchi, M. Neumann, and M. Zoppi, Phys. Rev. A **36,** 2440 (1987)].

ical properties are reduced according to rules concerning the strength and range of the interatomic interactions. For solid-state properties, one such reduction simply employs a characteristic temperature, Θ. Figure 7 shows reduced $\langle E_k \rangle$ values for Ne, Ar, Kr, and Xe on a common plot versus the reduced temperature. The Ne data neatly show the transition to ground-state conditions.

Solid Ar has considerable anharmonicity. For example, its thermal expansion is so large that at melting its isobaric heat capacity C_p is about 50% larger than its isochoric heat capacity C_v, and near melting the lattice C_v itself is smaller than $3R$ [38]. Whether this anharmonicity will be shown in DINS measurements of the deviation of $\langle E_k \rangle$ from classical values, as the temperature is reduced, is under investigation [37].

2. Ne as Intermediate Case

Ne has mass and intermolecular potential values between those of He and the heavier noble gases. It serves as a bridge between the behavior of He as a system dominated by quantum effects (including the effects of nuclear statistics upon macroscopic properties) and the behavior of Ar, Kr, and Xe as systems in some respects not too different from usual solids and liquids.

Figure 8 shows a measurement on liquid natural Ne at 35 K. Such DINS data on 35 K liquid Ne samples at two different densities (different applied pressures) show that $\langle E_k \rangle$ is only 2.6 ± 0.2 K (or 4%) higher for the liquid having a 9% higher macroscopic density [39]. (Compare the much larger expected difference (14) for a quantum solid.) This relative lack of density dependence shows that a 35 K liquid Ne exhibits only small quantum effects.

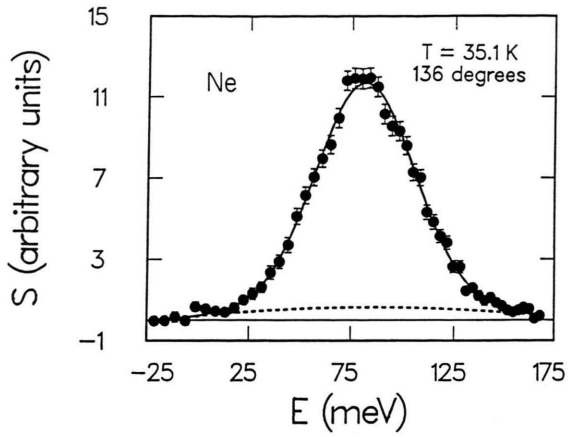

Fig. 8. DINS peak for liquid Ne at 35.1 K and density 34.5 atoms nm^{-3}, for an incident neutron energy of 498 meV [39]. Sample-dependent background is represented by a quadratic polynomial (dashed) included in the fitting of a Gaussian peak to the scattering at the fixed angle of 136°. For other Ne samples under similar conditions, the instrumental resolution and sample-dependent effects are similar, which allows precise comparison of differences between $S(\phi, \omega)$ data sets between samples.

On the other hand, in contrast to the results of Table 2, the presence of measurable density dependence at fixed 35 K indicates that Ne is not classical. For the two densities concerned, precise data are available from which the pair distribution $g(r)$ can be obtained [40]. The two radial distributions first peak at essentially the same values of internuclear separation, whereas these first peaks have significantly different amplitudes; that is, in the liquids of different macroscopic density, the shells of nearest neighbours have essentially the same radius, but they contain different average numbers of atoms. In the liquid of higher density, the atoms are more confined.

A further density dependence can be seen by comparing $\langle E_k \rangle$ values for liquid Ne and solid Ne [41] samples, both near the triple-point temperature of 24.6 K. The liquid sample was 16% less dense than the solid, and its measured value of $\langle E_k \rangle$ was 10% lower. No calculated values are yet available for comparison with these data. It is interesting to note that for solid Ne, $\langle E_k \rangle$ is about 60% of the total ground-state energy, as found for solid para-H_2 [23]. These two solids therefore have comparable lattice anharmonicity.

Because of the availability of $g(r)$ data and because its pair potential is well-known, liquid Ne is a promising system for investigation of final-state effects as illustrated in Fig. 3, and this study is in progress [37].

C) Systems with Internal Degrees of Freedom

Results about $\langle E_k \rangle$ from para-H_2 have already been discussed above in Sect. III.A. The para-H_2 system is an interesting prototype for the study of other effects [42]. The earliest neutron scattering experiments on molecular H_2, carried out to elucidate the strong n–p interaction, never had the resolution to measure $S(Q, \omega)$ directly. With chopper spectrometers, this is now possible, at least for para-H_2, which has a simpler spectrum than ortho-H_2. Herwig's results [43, 44] agree very well with refined calculations for the gas [45].

For such a system, (1) becomes

$$\frac{d^2\sigma}{d\Omega\, d\omega} = (k_f/k_i) \sum_m b_{0m}^2 S_{0m}(Q, \omega)\,, \tag{13}$$

where b_{0m} is the scattering length, and (2) becomes

$$S_{0m}(\boldsymbol{Q}, \omega) = f_{0m}(\boldsymbol{Q}) \int n(\boldsymbol{p})\, \delta\left(\omega - \frac{E_e}{\hbar} - \boldsymbol{Q}\cdot\boldsymbol{p}/M\right) d\boldsymbol{p}\,, \tag{14}$$

where $f_{0m}(\boldsymbol{Q})$ is the form factor associated with internal bound state m and E_e is the total molecular excitation energy

$$E_e = (\hbar^2 Q^2/2M) + E_m = E_r + E_m\,, \tag{15}$$

E_m being the energy to excite the mth bound molecular state. When for H_2 the initial state is $J = 0$ (para-H_2), successive peaks in the neutron spectrum correspond to final states $J = 1$, 3, 5, etc., provided the incident-neutron energy is insufficient to dissociate the H_2 molecule. These form factors $f_{0m}(Q)$ have pronounced dependence upon Q; for a given transition, they rise then fall. Owing to the excitation of higher molecular rotational states and the factors $f_{0m}(Q)$, which cut off the response at high Q, the amount of translational momentum transfer is limited. Nevertheless, it appears that the impulse approximation does apply.

In condensed H_2 the internal dynamics of vibration and rotation is weakly coupled to translational motion of the center of mass, so that the assumptions of Sect. I are well satisfied. Indeed, a DINS study of condensed para-H_2 reveals details such as centrifugal effects on the energy of successively higher rotational states [23], details which were neglected in the calculations [45]. As noted above, to simplify spectral analysis one can prepare the H_2 in the $J=0$ state (using a paramagnetic catalyst). Doing so also prepares a system in which

only central intermolecular forces are operative in the initial scattering state.

For a complex spectrum such as that of H_2, each peak is broadened by a common amount dependent upon the *initial* state $n(p)$. For such a spectrum the convenience of simple y-scaling in data analysis is lost, because of (15). But at a given scattering angle or given Q, there is a redundancy useful in extracting the value of the line-broadening (that is, the value of $\langle E_k \rangle$) as one fits the spectrum knowing the broadening is common to all peaks and using information such as the calculated $f_{0m}(Q)$'s. Note that although the increase of $\langle E_k \rangle$ at higher densities shown in Fig. 5 corresponds to massive broadening and overlapping in the H_2 spectrum, this overlapping could nevertheless be treated using knowledge of the basic spectrum.

D) Guest–Host Interactions

Condensed noble gases have long been used as transparent matrices for optical absorption, Raman, NMR, and ESR studies of embedded molecules and radicals [46]. The local atomic configuration and the center-of-mass translational motion of the molecules was seldom an issue, however, until concerns appeared with the extension of work into the VUV and XUV and the consideration of lighter elements [47].

Molecular H_2 has been extensively studied as an impurity in noble-gas solids and liquids. Center-of-mass vibrational frequencies have sometimes been derived incidental to other spectral studies, but the first direct (DINS) measurements were made by Herwig and coworkers on para-H_2 in Ar [43, 48]. This is a favorable case, because the dilute H_2 is a strongly scattering substitutional solute in the host fcc Ar crystal, which itself is a relatively weak scatterer. Figure 9 shows the measured scattering of neutrons of incident energy 500 meV, below the 517 meV threshold of the first intramolecular vibrational excitation of H_2. The domain of energy, E, and wave-vector transfer, Q, is bounded by kinematic limits; the data are broadened by instrumental resolution. In Fig. 9 the smooth, slowly curved (high mass) ridge in the rear is that of the host Ar; the peaks show H_2 transitions to the levels $J=1$, 3, and 5, respectively. From such data at different temperatures, the $\langle E_k \rangle$ of H_2 shows a) approach at low temperature to the ground-state vibrational energy of this light solute, b) high-temperature values that can be compared to those of the host Ar, and c) an intermediate region of smooth transition.

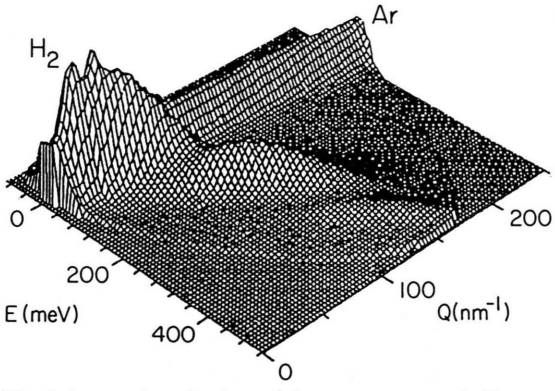

Fig. 9. Internal excitation of the target system is illustrated for para-H_2 [48]. Guest molecules in the condensed system are prepared in the state $J=0$. Incident neutrons excite the rotational states $J=1$, 3, and 5, visible as the three peaks modulated by the form factors $f_{0m}(Q)$ of (14). (Some statistical noise makes the $J=1$ peak irregular.) The weakly-scattering host Ar scatters along the ridge in the background, curved along $E=\hbar^2 Q^2/2M$, where M is the Ar mass.

DINS thus joins and complements other techniques, such as μeV neutron tunneling spectroscopy and those mentioned above, in the study of excitations in mixed systems. Here again, sophisticated simulations are becoming available of guest–host dynamics [49], for quantitative comparison with experiments.

V. Conclusion

The first generation of neutron Compton profile studies at high Q, on prototype systems composed of condensed gases, has verified the general principles of the technique. For several systems, theorists using PIMC and other sophisticated methods have apparently reduced their statistical uncertainties below the uncertainties present in first-generation neutron Compton measurements. A second generation of experimental studies, with improved treatment of instrumental resolution and with improved statistics, is yielding explicit results on final-state effects. These promise refined comparison with such calculations.

Acknowledgements

The experimental work reported here benefited from use of the Intense Pulsed Neutron Source at Argonne National Laboratory. This facility is funded by the U.S. Department of Energy, BES-Materials Sciences, under Contract W-31-109-ENG-38. The author is happy to acknowledge constructive comments by the editor in the course of publication.

[1] Final results appear in: H. A. Geiger and E. Marsden, Phil. Mag. **25,** 604 (1913).
[2] E. Rutherford, Phil. Mag. **21,** 669 (1911).
[3] A. H. Compton, Phys. Rev. **21,** 715 (1923); **22,** 409 (1923).
[4] J. W. M. DuMond, Revs. Mod. Phys. **5,** 1 (1933).
[5] S. W. Lovesey, Theory of Scattering from Condensed Matter, Clarendon Press, Oxford 1984, Vol. 1.
[6] P. C. Hohenberg and P. M. Platzman, Phys. Rev. **152,** 198 (1966).
[7] G. B. West, Physics Reports **18,** 263 (1975).
[8] V. F. Sears, Phys. Rev. B **30,** 44 (1984).
[9] A. Belić and V. R. Pandharipande, Phys. Rev. B **39,** 2696 (1989).
[10] See, for example: Momentum Distributions (R. N. Silver and P. E. Sokol, eds.), Plenum Press, New York 1989.
[11] P. Martel, E. C. Svensson, A. D. B. Woods, V. F. Sears, and R. A. Cowley, J. Low Temp. Phys. **23,** 285 (1976).
[12] T. R. Sosnick, W. M. Snow, R. N. Silver, and P. E. Sokol, Phys. Rev. B **43,** 216 (1991). – K. W. Herwig, P. E. Sokol, W. M. Snow, and R. C. Blasdell, Phys. Rev. B **44,** 308 (1991).
[13] C. G. Windsor, Pulsed Neutron Scattering, Taylor & Francis Ltd., London 1981.
[14] R. O. Hilleke, Ph.D. Thesis, University of Illinois at Urbana-Champaign, 1983 (unpublished).
[15] The instrument in this case was LRMECS at the Argonne IPNS; see C. K. Loong, S. Ikeda, and J. W. Carpenter, Nucl. Instrum. Methods A **260,** 381 (1987).
[16] R. C. Blasdell (to be published).
[17] P. A. Seeger, A. D. Taylor, and R. M. Brugger, Nucl. Instrum. Methods A **240,** 98 (1985). – D. N. Timms, M. J. Cooper, R. S. Holt, and P. Postorino, Nucl. Instrum. Methods A **294,** 509 (1990).
[18] P. Postorino, F. Fillaux, J. Mayers, J. Tomkinson, and R. S. Holt, J. Chem. Phys. **94,** 4411 (1991).
[19] A. C. Evans, J. Mayers, D. N. Timms, and M. J. Cooper, Z. Naturforsch. **48a,** 425 (1993).
[20] See H. R. Glyde and E. C. Svensson, in: Neutron Scattering in Condensed Matter Research (K. Skold and D. L. Price, eds.), Academic Press, New York 1987, Vol. 23 B, Chapt. 13. – R. S. Holt, L. M. Needham, and M. P. Paoli, Phys. Letters A **126,** 359 (1988) and Portgal. Phys. **19,** 363 (1988); and Ref. [10].
[21] R. O. Hilleke, P. Chaddah, R. O. Simmons, D. L. Price, and S. K. Sinha, Phys. Rev. Lett. **52,** 847 (1984).
[22] M. Nielsen, Phys. Rev. B **7,** 1626 (1973).
[23] W. E. Langel, D. L. Price, R. O. Simmons, and P. E. Sokol, Phys. Rev. B **38,** 275 (1988).
[24] K. W. Herwig, J. C. Gavilano, M. C. Schmidt, and R. O. Simmons, Phys. Rev. B **41,** 96 (1990).
[25] J. K. Krause and C. A. Swenson, Solid State Commun. **31,** 833 (1979). – J. K. Krause, Ph.D. Thesis, Iowa State University, 1978 (unpublished).
[26] See Fig. 8 in R. O. Simmons, Can. J. Phys. **65,** 1401 (1987).
[27] T. A. Bruce, Phys. Rev. B **5,** 4170 (1972).
[28] H. A. Mook, Phys. Rev. Lett. **32,** 1167 (1974).
[29] P. E. Sokol, R. O. Simmons, D. L. Price, and R. O. Hilleke, in: Proc. XVII Conf. on Low Temperature Physics (U. Eckern, A. Schmid, W. Weber, and H. Wuhl, eds.), North-Holland Publ. Co., Amsterdam 1984, p. 1213.
[30] R. C. Blasdell, D. M. Ceperley, and R. O. Simmons, Z. Naturforsch. **48a,** 433 (1993).
[31] D. Ceperley, in: Momentum Distributions (R. N. Silver and P. E. Sokol, eds.), Plenum Press, New York 1989, p. 71.
[32] See M. P. Paoli and R. S. Holt, J. Phys. C: Solid State Physics **21,** 3633 (1988) and Portgal. Phys. **19,** 365 (1988) for data on $n(p)$ anisotropy in pyrolytic graphite, and Ref. [18] for a report on hydrogen bonds in a chemical compound.
[33] P. E. Sokol, D. A. Peek, R. O. Simmons, D. L. Price, and R. O. Hilleke, Phys. Rev. B **33,** 7787 (1986).
[34] M. Zoppi and M. Neumann, Phys. Rev. B **43,** 10242 (1991).
[35] See for example the shadow wave function GFMC method of S. A. Vitiello, K. J. Runge, G. V. Chester, and M. H. Kalos, Phys. Rev. B **42,** 228 (1990) and the variational path-integral theory of S. Liu, G. K. Horton, and E. R. Cowley, Phys. Rev. B **44,** 11714 (1991).
[36] D. A. Peek and R. O. Simmons, J. Chem. Phys. **94,** 3169 (1991).
[37] M. A. Fradkin, S.-X. Zeng, and R. O. Simmons, Bull. Amer. Phys. Soc. **36,** 772 (1991) and Z. Naturforsch. **48a,** 438 (1993).
[38] F. Haenssler, K. Gamper, and B. Serin, J. Low Temp. Phys. **3,** 23 (1970).
[39] D. A. Peek, M. C. Schmidt, I. Fujita, and R. O. Simmons, Phys. Rev. B **45,** 9671 (1992).
[40] L. A. de Graaf and B. Mozer, J. Chem. Phys. **55,** 4967 (1971).
[41] D. A. Peek, I. Fujita, M. C. Schmidt, and R. O. Simmons, Phys. Rev. B **45,** 9680 (1992).
[42] R. O. Simmons and P. E. Sokol, Physica **136B,** 156 (1986).
[43] K. W. Herwig and R. O. Simmons, in: Momentum Distributions (R. N. Silver and P. E. Sokol, eds.), Plenum Press, New York 1989, p. 203.
[44] K. W. Herwig and R. O. Simmons, Molecular Phys. **75,** 1393 (1992).
[45] J. A. Young and J. U. Koppel, Phys. Rev. **135A,** 603 (1964).
[46] M. L. Klein, ed., Inert Gases: Potentials, Dynamics, and Energy Transfer in Doped Crystals, Springer-Verlag, Heidelberg 1984.
[47] See for example: Yu. I. Rybalko, E. V. Savchenko, and I. Ya. Fugol, Sov. J. Low Temp. Phys. **11,** 349 (1985).
[48] K. W. Herwig, R. C. Blasdell, and R. O. Simmons (to be published).
[49] B. Silvi, V. Chandrasekharan, M. Chergui, and R. D. Etters, Phys. Rev. B **33,** 2749 (1986).